BOLETIN DE LA SOCIEDAD ESPAÑOLA DE
Cerámica y Vidrio
www.elsevier.es/bsecv

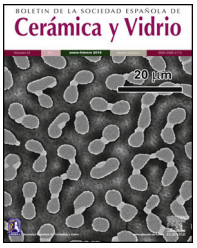

Original

Two-step doping approach releasing the piezoelectric response of $BiFeO_3$ bulk ceramics co-doped with titanium and samarium

Carlos Gumiel[a], *Mara S. Bernardo*[a,b], *Pablo G. Villanueva*[b], *David G. Calatayud*[b], *Marco Peiteado*[b], *Teresa Jardiel*[b,*]

[a] *POEMMA-CEMDATIC, ETSI Telecomunicación (UPM), Avd. Complutense 30, 28040 Madrid, Spain*
[b] *Department of Electroceramics, Instituto de Cerámica y Vidrio (CSIC), Kelsen 5, 28049 Madrid, Spain*

ARTICLE INFO

Article history:
Received 3 June 2019
Accepted 1 July 2019
Available online 19 July 2019

Keywords:
BiFeO3
Processing
Microstructure
Electrical conductivity
Piezoelectricity

ABSTRACT

The conventional solid state processing of bulk Ti,Sm co-doped $BiFeO_3$ ceramics typically produces a complex micro-nanostructure which exhibits an effective decrease of the leakage conductivity. This same nanostructured configuration however confines the mobility of the ferroelectric domains and in this way the potential piezoelectric response of the formulated composition remains restrained. Hereby, a two-step doping strategy based on a simple surface modification approach is proposed which eventually allows for suitably engineering the microstructural development of the material, leading to a coarsened configuration where the conductivity is kept in low levels while the piezoelectric response is satisfactorily released for practical purposes.

Desarrollo de una estrategia de dopado en dos etapas para liberar la respuesta piezoeléctrica de cerámicas en volumen de $BiFeO_3$ co-dopado con titanio y samario

Palabras clave:
$BiFeO_3$
Procesamiento
Microestructura
Conductividad eléctrica
Piezoelectricidad

RESUMEN

El procesamiento convencional en estado sólido de materiales cerámicos en volumen de $BiFeO_3$ co-dopado con Ti y Sm, típicamente produce una compleja micro-nanoestructura que permite una reducción efectiva de la conductividad eléctrica del material (corrientes de fuga). Sin embargo, esta misma configuración nano-estructurada también reduce la movilidad de los dominios ferroeléctricos y por ello, la potencial respuesta piezoeléctrica de la composición formulada permanece confinada. En este trabajo se propone el empleo

* *Corresponding author.*
E-mail address: jardiel@icv.csic.es (T. Jardiel).
https://doi.org/10.1016/j.bsecv.2019.07.002

de una estrategia de dopado en dos etapas, basada en una sencilla aproximación de modificación superficial, con la cual es posible diseñar y controlar adecuadamente el desarrollo microestructural del sistema, dando lugar a un engrosamiento de la microestructura que permite mantener la conductividad del material en bajos niveles al tiempo que libera satisfactoriamente su respuesta piezoeléctrica.

Introduction

In addition to its well-investigated multiferroic possibilities, single phase $BiFeO_3$ also withstands as a promising candidate for lead-free piezoelectric applications [1–4]. The stereochemically active lone-pair electrons of Bi^{3+} are responsible for the displacement of these cations along the [111] pseudo-cubic axis of the perovskite structure, bringing about a non-centrosymmetric polarization which results in the piezoelectric property [5–7]. However, although such displacements of the A-sites are rather large (relative to the centrosymmetric cubic perovskite structure), the obtained polarizations are indeed too small in the pure $BiFeO_3$ compound and so doping becomes a compulsory option [8–12]. Rare earths are among the most helpful dopants in this sense, since they can lead to the formation of a morphotropic phase boundary (MPB) when replacing the Bi^{3+} ions in the A-sites [13–15]. Moreover, a material in the vicinity of the phase boundary usually exhibits significant physical responses in reaction to relatively weak external stimulus [16–19]. Specifically, the isovalent substitution of bismuth for samarium, $Bi_{1-x}Sm_xFeO_3$, can produce a significant enhancement of the piezoelectric properties in the compositional range $0.12 \leq x \leq 0.16$, where a polar-to-non-polar MPB has been postulated by several authors [2,16,20–24]. Unfortunately, the incorporation alone of samarium cannot completely suppress the intrinsic conductivity of the material (high leakage current) and so the electromechanical properties of Sm-modified $BiFeO_3$ bulk ceramics typically remain inaccessible [25–27]. The simultaneous addition of titanium may unblock this condition [28–31]. Upon Ti-doping a specific micro-nanostructure is generated within the $BiFeO_3$ bulk material which is then composed by small grains of nanometric size separated by titanium-rich areas [32,33]. Just a limited concentration of Ti^{4+} is incorporated into the perovskite crystal lattice and the titanium-rich interfaces behave like highly resistive layers, increasing the direct-current (dc) resistivity of the whole material [32,34]. From the point of view of piezoelectric functionality, there is however one limiting setback in this scenario: the nanostructured configuration severely impedes the mobility of the ferroelectric domains, hence leading to a low degree of polarization and a poor piezoelectric response [35]. An intermediate situation in which such nanostructure would be reasonably coarsened while preserving the structural/electronic configuration of the formulated composition, would be ideal, and here is where processing becomes a valuable tool: we can use processing to purposely engineer the microstructure of the material and further capitalize on its intrinsic properties. Aiming this goal, in this contribution we have devised a specific a two-step doping processing approach that, by deliberately coarsening the microstructure of the $BiFeO_3$ co-doped system, allows for an effective domain mobility while having a low conductivity, hence giving access to a functional piezoelectric response.

Experimental procedure

Ceramic powders with nominal composition $Bi_{0.88}Sm_{0.12}Fe_{0.95}Ti_{0.05}O_{3.025}$ (BSFTO hereafter) were prepared using two different methodologies. In a first routine, a conventional solid state process is practiced by mixing the corresponding amounts of the oxide precursors, Bi_2O_3 (Aldrich, 99.9%), Fe_2O_3 (Sigma–Aldrich, >99%), Sm_2O_3 (Aldrich 99.9%) and TiO_2 (anatase structure, Sigma–Aldrich, >99%), and subjecting them to 2 h of attrition milling with YSZ (yttria-stabilized zirconia) balls and ethanol as liquid medium. As described elsewhere [36], the dried mixture is sieved under a 100 μm mesh and heated up to 800 °C during 2 h in order to produce the synthesis of the perovskite phase. The obtained solid is again milled to crush the as-formed agglomerates and aggregates (as much as possible), and once dried it is again sieved to render a loose powder ready for sintering. The second methodology also starts from the standard solid state routine, although the incorporation of the dopants is produced in two steps. In a first step just the oxide precursor of samarium is mixed (milled) with those of bismuth and iron and heated at 800 °C/2 h for the synthesis of a nominal Sm-doped $BiFeO_3$ material. Like in the previous method the obtained solid is fragmented with a new milling stage, but once dried it is now dispersed in absolute ethanol. The corresponding amount of titanium (IV) isopropoxide (Aldrich, 99.9%) is then dripped into the dispersion while stirring the mixture with a high speed disperser (IKA Ultra-Turrax T25). After 15 min at 11,000 rpm, the mixture is dried and sieved (100 μm), yielding also a ready-to-sinter ceramic powder. This second approach will produce a sort of titanium-rich coating on the surface of the previously formed Sm-doped bismuth ferrite particles, and as a straight consequence a different grain growth evolution is to be expected. The FESEM and TEM images in Fig. 1 evidence how this coating looks like in the obtained powder, which hereafter will be referred as BSFTO-m (*m* stands for surface modified powder).

Samples of the two powders were next sintered in the form of isostatically pressed pellets ($\phi = 0.8$ cm, $P = 250$ MPa). An optimum density above 95% of the $BiFeO_3$ theoretical density was attained under the following sintering conditions: 925 °C during 8 h for the BSFTO powder and 1000 °C during 2 h for the modified BSFTO-m material. Notice that in both compositions

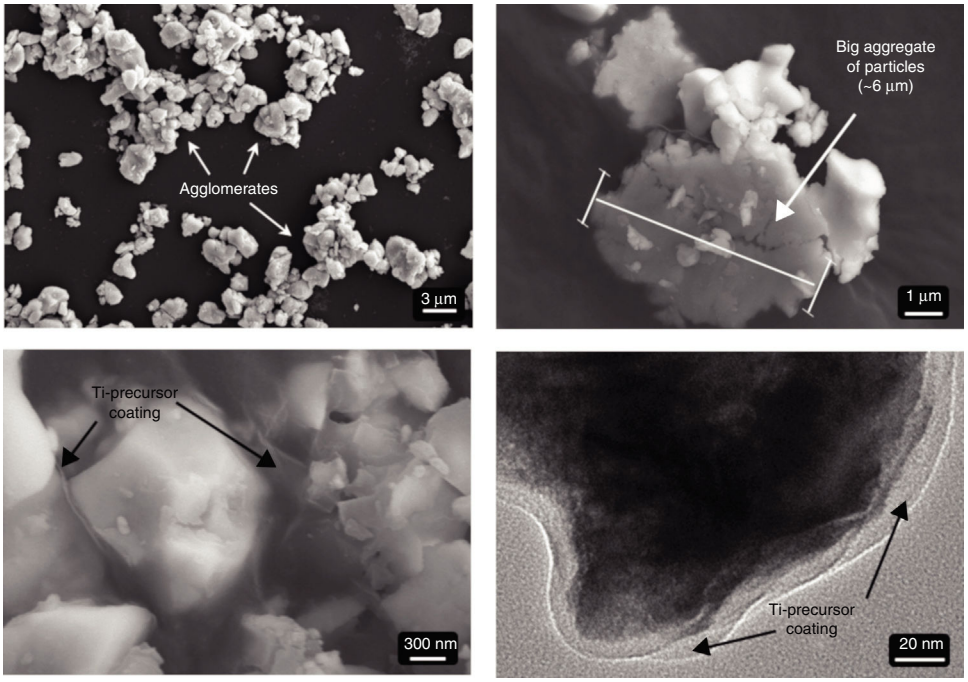

Fig. 1 – FESEM and TEM images of the BSFTO-m powder, right after the impregnation with titanium isopropoxide. Individual particles, agglomerates and aggregates persisting after the previous milling step, are all fully coated by a thin layer of the liquid Ti-precursor.

the sintering temperature is well-above the peritectic point of pure BFO, but this never affects the distribution, purity and/or stoichiometry of the crystallized phases. For comparison issues, the following 3 reference compositions were as well prepared applying the conventional solid state process: undoped $BiFeO_3$ (BFO), Ti-doped $BiFeO_3$ (BFTO) and Sm-doped $BiFeO_3$ (BSFO).

The structural characterization of the sintered ceramics was carried out by means of X-ray diffraction (XRD) measurements on a Bruker D8 Advance diffractometer using CuKα radiation; patterns were collected between $2\theta = 15^\circ$ and $2\theta = 65^\circ$, in steps of 0.015° and with a counting time of 0.5 s per step. The FullProf 2k program [37] and its graphical interface WinPLOTR [38] were operated to refine the experimental XRD data (Le Bail method). The densification behavior of the sintered pellets was followed by measuring the Archimedes density in water. The microstructure of the samples was observed on polished and chemically (aq. diluted HCl) etched surfaces by Field Emission Scanning Electron Microscopy (FESEM), using a Hitachi S-4700 microscope equipped with EDS. Transmission Electron Microscopy (TEM) was used to further characterize the synthesized powders, using a JEOL 2100F microscope (TEM/STEM) operating at 200 kV and equipped with a field-emission electron gun. Grain size measurements were evaluated from the FESEM micrographs by an image processing and analysis program (Leica) that measures the surface of each $BiFeO_3$ grain and transforms its irregularly shaped area into a circle of equivalent diameter. The electrical characterization was carried out on Ag-Pd electroded discs. Direct-current (dc) conductivity measurements were performed at 220 °C in a voltage range between 20 V and 200 V, using a Keithley Model 2410 power multimeter. The ferroelectric loops and the piezoelectric coefficients d_{31} and d_{33} were determined by respectively using a RT6000HVS hysteresimeter (Radiant technologies) and an impedance analyzer (Agilent 4294A) with the resonance-antiresonance technique.

Results and discussion

The XRD characterization revealed an almost pure $BiFeO_3$ composition for all the doped formulations after the sintering stage. Fig. 2 specifically shows the 2θ region between 31° and 33° for the undoped material and the two co-doped samples. For the parent BFO composition this area shows a double *hkl* reflection profile which is attributed to the *R3c* rhombohedral phase of $BiFeO_3$, Fig. 2a. In the doped samples the two Bragg peaks of the *R3c* phase have characteristically converged into a single *hkl* reflection [22,33], coinciding also with the entering of the *Pbam* orthorhombic symmetry of $BiFeO_3$, Figs. 2b and c. Both phases indeed constitute the mentioned MPB of the Sm-doped $BiFeO_3$ formulation, which is consonance with the Sm-content used for this study ($x = 0.12$, i.e. right in the edge of the reported MPB region [20–24]). The refined cell parameters of the co-doped materials are listed in Table 1, where they are compared with the undoped and the mono-doped compositions of reference. These data confirm that whereas titanium is hardly incorporated to the *R3c* lattice, samarium more easily gets into the perovskite structure, leading to a considerable decrease of the primitive cell volume. But moreover, the calculations also evidence that at this point the processing routine has no major influence on the structural evolution of the materials, all the

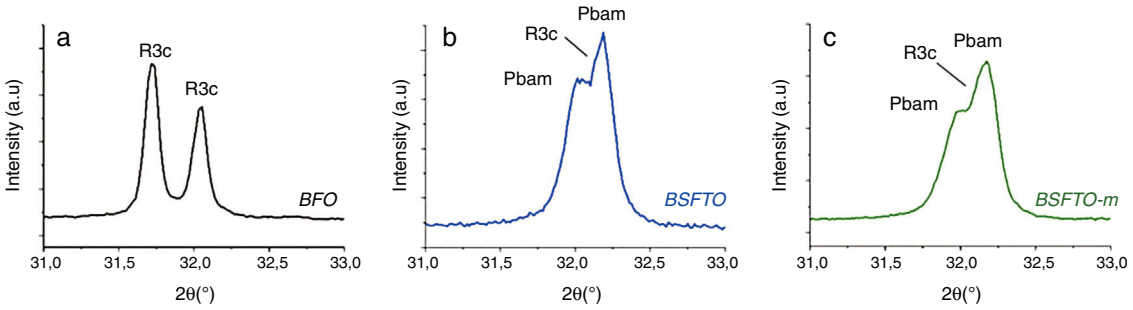

Fig. 2 – XRD patterns in the 31–33° 2θ region for the (a) BFO, (b) BSFTO and (c) BSFTO-m sintered samples, showing the presence of the rhombohedral *R3c* and the orthorhombic *Pbam* phases of $BiFeO_3$.

Table 1 – Lattice parameters, volume of the *R3c* primitive cell and reliability factors for the five sintered samples, as obtained from the Le Bail structural fitting of the corresponding XRD patterns.

	$a = b$ (Å)	c (Å)	V (Å^3)	R_p	R_{wp}
BFO	5.575 (2)	13.860 (5)	373.05 (3)	5.9	10.3
BFTO	5.577 (2)	13.840 (5)	372.75 (3)	3.8	5.4
BSFO	5.567 (2)	13.780 (7)	369.85 (4)	4.8	6.6
BSFTO	5.58 (2)	13.69 (9)	369.1 (3)	9.5	18.0
BSFTO-m	5.57 (1)	13.77 (5)	369.7 (1)	6.6	10.0

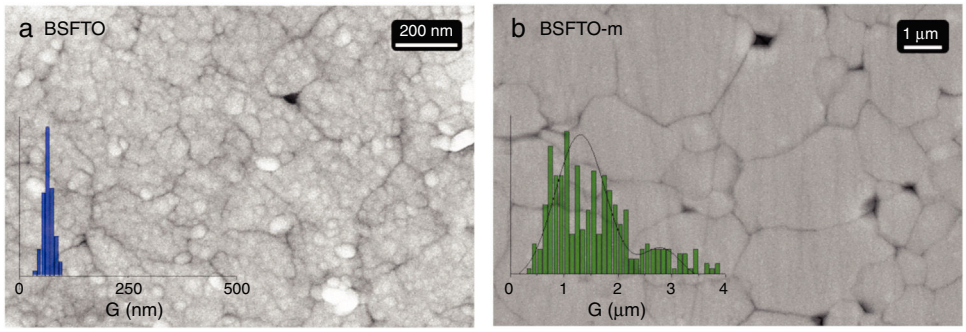

Fig. 3 – Main microstructural features of the co-doped samples: FESEM image and grain size distribution of (a) the BSFTO conventional sample sintered at 925 °C/8 h and (b) the BSFTO-m sample sintered at 1000 °C/2 h.

Sm-containing samples practically displaying the same lattice parameters.

The FESEM images in Fig. 3 however evidence the microstructural differences between the two tested procedures. The conventionally processed BSFTO sample displays the described micro-nanostructure which is obtained upon Ti-doping, composed of uniformly dispersed nanograins with a very narrow size distribution (average size around 50 nm, Fig. 3a). As reported, this is a straight consequence of the segregation of titanium to the grain boundaries, in a diffusion-controlled process which leads to a solute-drag effect that inhibits the growth of the $BiFeO_3$ grains [32,39]. On the contrary, the surface modified BSFTO-m composition shows the projected coarsened disposition in which the $BiFeO_3$ grains have noticeably increased their size. The histogram depicted inside the FESEM image of Fig. 3b also evidences a significantly broader grain size distribution, pointing even to a bimodal-like tendency where most of the grains now display an average size close to 1.2 microns, but larger grains of around 3 micros and beyond are also frequently observed. Visibly, the modification introduced in the "standard" processing of the material is behind this microstructural alteration, and it should be attributed to the fact that the titanium being incorporated in the second step is not accessing the pre-synthesized powders in a homogeneous way. A plausible mechanism is described as follows: In the BSFTO material, the Ti-precursor is homogenously mixed with the other precursors from the very beginning, and thus during the synthesis stage it is well distributed all over the material. As described, right after the synthesis a new milling process is conducted that crushes the obtained solid into a mixture of de-agglomerated particles, some persistent agglomerates and some aggregates which cannot be broken during the milling (not enough energy to fragment them). But even then, the titanium is present everywhere in this BSFTO powder, i.e. in the discrete units but also inside the agglomerates and the aggregates of particles; hence, upon the subsequent sintering it can efficiently inhibit the growth of the $BiFeO_3$ grains, segregating to all the grain boundaries to exert the mentioned solute-drag constraining effect [32,39], and eventually producing

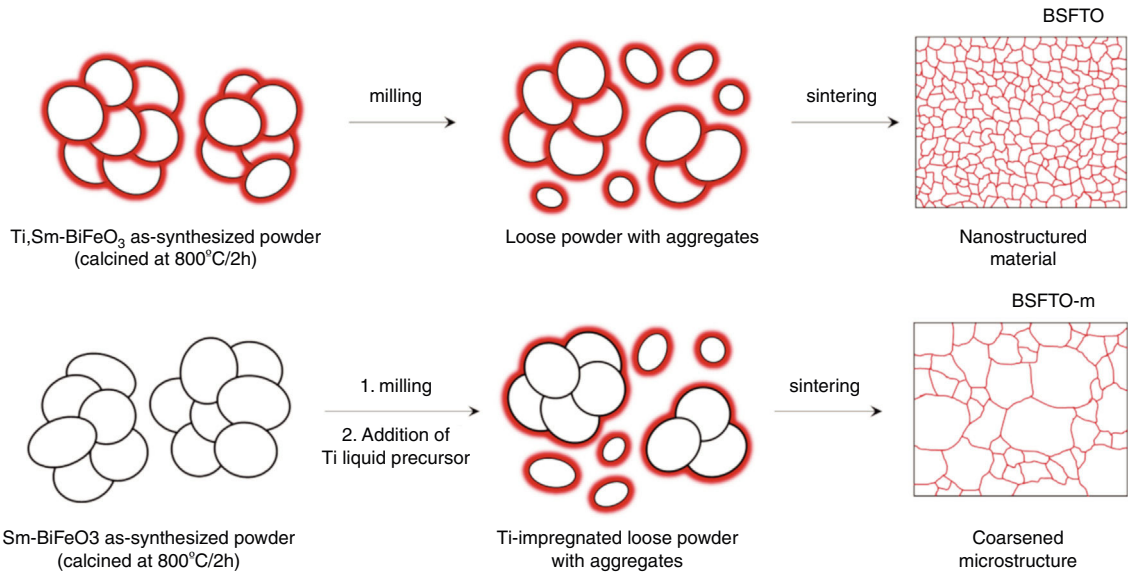

Fig. 4 – Schematic diagram illustrating the distinct microstructural evolution experienced by the two co-doped samples as a consequence of the different incorporation of the Ti dopant (different processing route). The red coloration denotes a Ti-enriched region (see further explanation in the text).

the observed nanostructure, Fig. 3a. In the surface modified BSFTO-m material, however, no titanium is present during the initial synthesis at 800 °C/2 h. It is later incorporated after the re-milling stage, as a liquid that impregnates the fragmented mixture of particles, agglomerates and aggregates (Fig. 1), and so we can initially presume that we have no titanium in the inner areas of those agglomerates and aggregates. Moreover, the situation is not likely to change substantially during the sintering, provided that titanium generally has a poor inertia to diffuse [40]. Consequently, upon sintering, this worst (less homogeneous) distribution of titanium trough the material will allow many of the existing agglomerates and aggregates of particles to freely densify without further inhibition, leading to the anticipated coarsening of the microstructure in which grains have unevenly grown up to two orders of magnitude, Fig. 3b. The sketch depicted in Fig. 4 has been conceived to better picture this distinct microstructural evolution of the two co-doped compositions; as indicated, a red coloration is used which highlights the differentiating Ti-enriched regions being generated by the two processing routes under examination in this study.

Fig. 5 shows the results of the *dc* conductivity measurements performed on the two co-doped samples and compared with the BSFO reference composition which contains no titanium. These measurements were conducted by registering the current density as a function of the (applied) electric field and, as depicted, in all cases a linear behavior is observed within the whole working range, which allows for assuming an ohmic conduction in the three tested materials. The *dc* resistivity values were then estimated from the slope of the straight line obtained by a least-square fitting methodology, rendering resistivities in the range of 10^4 Ω cm for the BSFO material, 10^7 Ω cm for the BSFTO sample and 10^6 Ω cm for the BSFTO-m surface modified material. As discussed in the introduction, doping only with samarium cannot completely suppress the

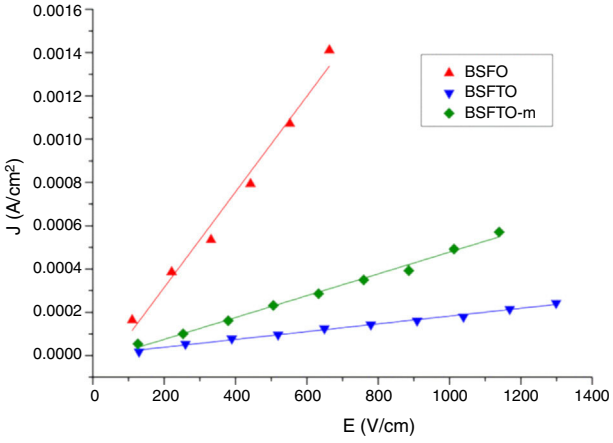

Fig. 5 – Evolution of the current density as a function of the applied *dc* electric field (i.e., *dc* conductivity) for the BSFO, BSFTO and BSFTO-m sintered materials.

intrinsic conductivity of $BiFeO_3$, explaining why the BSFO composition is by far the most conductive. The conductivity significantly decreases when the titanium is incorporated to the starting formulation; quite largely for the conventionally processed BSFTO sample, and less pronouncedly for the surface modified BSFTO-m material. The different size of the $BiFeO_3$ perovskite grains is behind this dissimilar behavior. In both samples the titanium segregates to the grain boundaries, which then behave as insulating barriers that control the macroscopic conductivity of the material [32]. Indeed, the formation of highly resistive layers by donor/acceptor interfacial segregation is the basis for important boundary-layer devices (PTCR thermistors, internal boundary layer capacitors, varistors), which exhibit the following relation between the electrical behavior and the grain size: the conductivity rises as

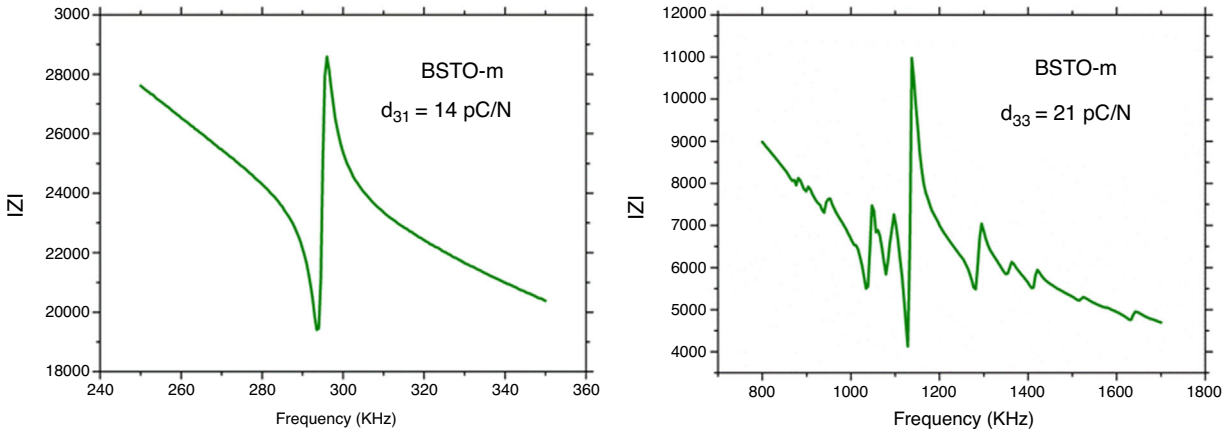

Fig. 6 – Piezoelectric coefficients d_{31} and d_{33} for the BSFTO-m sample as measured by the resonance-antiresonance methodology.

the grain size increases, provided this implies a lower amount of (insulating) grain boundaries [41–44]. This is exactly the relation that we observe in the BSFTO-m composition, which has a coarsened microstructure (Fig. 3b) and, consequently, a higher conductivity than the BSFTO conventionally processed sample (Fig. 5). The point here is that this detrimental circumstance caused by the bigger size of the perovskite grains, may simultaneously have a positive counterbalance in the material's piezoelectric possibilities, this being the main goal of our investigation. The ferroelectric characterization of the co-doped samples was then attempted by means of polarization vs. electric field measurements, but no printable results were obtained since the corresponding P-E hysteresis loops were far from saturation. Subsequently, both samples were poled at poled at 60 kV/cm and 100 °C and the macroscopic piezoelectric response was assessed by the resonance-antiresonance method. The obtained results are very conclusive: as expected, the nanostructured configuration displayed by the $BiFeO_3$ nano-grains in the BSFTO conventionally processed material is a critical impediment for the mobility of the ferroelectric domains, in such a way that no piezoelectric coefficients could be measured for this sample; on the contrary, the bigger size of the perovskite grains in the surface modified BSFTO-m co-doped material allows for and increased domain mobility and hence releases the postulated piezoelectricity of this co-doped formulation, returning a d_{31} coefficient of $14{\cdot}10^{-12}$ C/N and a d_{33} of $21{\cdot}10^{-12}$ C/N, as depicted in Fig. 6.

Conclusions

In summary, the two-step doping strategy here proposed to produce bulk Ti,Sm co-doped $BiFeO_3$ ceramics, modifies the *conventional* microstructural development of the material and leads to a coarsened configuration that better capitalizes on the benefits provided by the two dopants: a low conductivity is yet preserved which results from the presence of titanium at the grain boundaries, but, simultaneously, the incorporation of samarium into the big perovskite grains allows for an enhanced domain mobility, subsequently releasing the piezoelectric potential of this specific composition.

Acknowledgements

This work was supported by the Spanish Ministry of Economy and Competitiveness (MINECO) through MAT2016-80182-R and MAT2014-59210-JIN projects. Dr. T. Jardiel acknowledges the European Science Foundation (ESF) and the Ramon y Cajal Program of MINECO for the financial support. Dr. D.G. Calatayud also acknowledges the Fundación General CSIC (ComFuturo Program) for the financial support.

REFERENCES

[1] J. Rödel, W. Jo, K.T.P. Seifert, E. Anton, T. Granzow, D. Damjanovic, Perspective on the development of lead-free piezoceramics, J. Am. Ceram. Soc. 92 (2009) 1153–1177.
[2] X. Chen, Y. Wang, Y. Yang, G. Yuan, J. Yin, Z. Liu, Structure, ferroelectricity and piezoelectricity evolutions of $Bi_{1-x}Sm_xFeO_3$ at various temperatures, Solid State Commun. 152 (2012) 497–500.
[3] M. Villegas, A.C. Caballero, T. Jardiel, C. Aragó, J. Maudes, I. Caro, Evaluation of piezoelectric properties if $Bi_4Ti_3O_{12}$-based ceramics at high temperature, Ferroelectrics 393 (2009) 44–53.
[4] T. Rojac, M. Makarovic, J. Walker, H. Ursic, D. Damjanovic, T. Kos, Piezoelectric response of $BiFeO_3$ ceramics at elevated temperatures, Appl. Phys. Lett. 109 (2016) 042904.
[5] G. Catalan, J.F. Scott, Physics and applications of bismuth ferrite, Adv. Mater. 21 (2009) 2463–2485.
[6] T. Jardiel, A.C. Caballero, J.F. Fernández, M. Villegas, Domain structure $Bi_4Ti_3O_{12}$ ceramics revealed by chemical etching, J. Eur. Ceram. Soc. 26 (2006) 2823–2826.
[7] T. Jardiel, A.C. Caballero, M. Villegas, Sintering kinetic of $Bi_4Ti_3O_{12}$ based ceramics, Bol. Soc. Esp. Ceram. Vidr. 45 (2006) 202–206.
[8] P. Ravindran, R. Vidya, A. Kjekshus, H. Fjellvag, O. Eriksson, Theoretical investigation of magnetoelectric behavior in $BiFeO_3$, Phys. Rev. B 74 (2006) 224412.
[9] C.H. Yang, D. Kan, I. Takeuchi, V. Nagarajan, J. Seidel, Doping $BiFeO_3$: approaches and enhanced functionality, Phys. Chem. Chem. Phys. 14 (2012) 15953–15962.
[10] V.A. Khomchenko, D.A. Kiselev, M. Kopcewicz, M. Maglione, V.V. Shvartsman, P. Borisov, W. Kleemann, A.M.L. Lopes, Y.G. Pogorelov, J.P. Araujo, R.M. Rubinger, N.A. Sobolev, J.M. Vieira,

A.L. Kholkin, Doping strategies for increased performance in $BiFeO_3$, J. Magn. Magn. Mater. 321 (2009) 1692–9168.
[11] M.S. Bernardo, T. Jardiel, M. Villegas, Synthesis and microstructural evolution of $BiFeO_3$ ceramics modified with ZnO, Bol. Soc. Esp. Ceram. Vidr. 49 (2010) 47–52.
[12] M.S. Bernardo, T. Jardiel, M. Peiteado, A.C. Caballero, Metastable nature of donor-doped $BiFeO_3$ obtained by mechanochemical synthesis, J. Ceram. Soc. Jpn. 124 (2016) 92–97.
[13] D. Arnold, Composition-driven structural phase transitions in rare-earth-doped $BiFeO_3$ ceramics: a review, IEEE Trans. Ultrason. Ferroelectr. Freq. Control. 62 (2015) 62–82.
[14] H. Tao, J. Lv, R. Zhang, R. Xiang, J. Wu, Lead-free rare earth-modified $BiFeO_3$ ceramics: phase structure and electrical properties, Mater. Des. 120 (2017) 83–89.
[15] C.S. Tu, C.S. Chen, P.Y. Chen, Y.L. Hsieh, R.R. Chien, V.H. Schmidt, K.C. Feng, H.W. Chang, Composition and thermal structural evolution in Pr modified bismuth ferrite near the morphotropic phase boundary, J. Alloy. Compd. 168 (2018) 903–913.
[16] J. Walker, P. Bryant, V. Kurusingal, C. Sorrell, D. Kuscer, G. Drazic, A. Bencan, V. Nagarajan, T. Rojac, Synthesis-phase-composition relationship and high electric-field-induced electromechanical behavior of samarium-modified $BiFeO_3$ ceramics, Acta Mater. 83 (2015) 149–159.
[17] S.D. Zhou, Y.G. Wang, Y. Li, H. Ji, H. Wu, Structural, magnetic and ferroelectric properties of Sm and Mn co-substituted $BiFeO_3$ ceramics with composition near the morphotropic phase boundary, Ceram. Int. 44 (2018) 13090–13096.
[18] Z. Liao, F. Xue, W. Sun, D. Song, Q. Zhang, J.F. Li, L.Q. Chen, J. Zhu, Reversible phase transition induced large piezoelectric response in Sm-doped $BiFeO_3$ with a composition near the morphotropic phase boundary, Phys. Rev. B 95 (2017) 214101.
[19] S. Adel, B. Cherifa, D.D. Elhak, B. Mounira, Effect of Cr_2O_3 and Fe_2O_3 doping on the thermal activation of un-polarized PZT charge carriers, Bol. Soc. Esp. Ceram. Vidr. 57 (2018) 124–131.
[20] C. Yu, G. Viola, D. Zhang, K. Zhou, V. Koval, A. Mahajan, R.M. Wilson, N.V. Tarakina, I. Abrahams, H. Yan, Phase evolution and electrical behavior of samarium-substituted bismuth ferrite ceramics, J. Eur. Ceram. Soc. 38 (2018) 1374–1380.
[21] J. Walker, H. Ursic, A. Bencan, B. Malic, H. Simons, I. Reaney, G. Viola, V. Nagarajan, T. Rojac, Temperature dependent piezoelectric response and strain-electric-field hysteresis of rare-earth modified bismuth ferrite ceramics, J. Mater. Chem. C 33 (2016) 7859–7868.
[22] J. Walker, H. Simons, D.O. Alikin, A.P. Turygin, V.Y. Shur, A.L. Kholkin, H. Ursic, A. Bencan, B. Malic, V. Nagarajan, T. Rojac, Dual strain mechanisms in a lead-free morphotropic phase boundary ferroelectric, Sci. Rep. 6 (2016) 19630.
[23] D.V. Karpinsky, I.O. Troyanchuk, A.V. Trukhanov, M. Willinger, V.A. Khomchenko, A.L. Kholkin, V. Sikolenko, T. Maniecki, W. Maniukiewicz, S.V. Dubkov, M.V. Silibin, Structure and piezoelectric properties of Sm-doped $BiFeO_3$ ceramics near the morphotropic phase boundary, Mater. Res. Bull. 112 (2019) 420–425.
[24] C. Gumiel, T. Vranken, M.S. Bernardo, T. Jardiel, A. Hardy, M.K. Van Bael, M. Peiteado, Thin film composites in the $BiFeO_3$-$Bi_4Ti_3O_{12}$ system obtained by an aqueous solution-gel deposition methodology, Bol. Soc. Esp. Ceram. Vidr. 57 (2018) 19–28.
[25] T. Rojac, A. Bencan, B. Malic, G. Tutuncu, J.L. Jones, J.E. Daniels, D. Damjanovic, $BiFeO_3$ ceramics: processing, electrical and electromechanical properties, J. Am. Ceram. Soc. 97 (2014) 1993–2011.
[26] G. Arya, J. Yogiraj, N.S. Negi, J. Shah, R.K. Kotnala, Observation of enhanced multiferroic, magnetoelectric and photocatalytic properties in Sm-Co codoped $BiFeO_3$ nanoparticles, J. Alloy Compd. 723 (2017) 983–994.
[27] P. Sharma, P. Saxena, A. Kumar, D. Varshney, Structural and multiferroic properties of $Bi_{0.885}Sm_{0.115}FeO_3$, J. Alloy Compd. 706 (2017) 609–615.
[28] P.K. Jha, P.A. Jha, P. Singh, R. Ranjan, R.K. Dwivedi, Sm/Ti co-substituted bismuth ferrite multiferroics: reciprocity between tetragonality and piezoelectricity, Phys. Chem. Chem. Phys. 19 (2017) 26285–26295.
[29] H. Mana-ay, J. Anthoniappen, C.S. Tu, R. Sarmiento Jr., C.S. Chen, P.Y. Chen, F.M. Ruiz, Improved microstructure and ferroelectric properties in B-site Ti^{4+}-substituted $(Bi_{0.86}Sm_{0.14})FeO_3$ polycrystalline ceramics, Mater. Chem. Phys. 225 (2019) 272–278.
[30] A. Anwar, M.A. Basith, S. Choudhury, From bulk to nano: a comparative investigation of structural, ferroelectric and magnetic properties of Sm and Ti co-doped $BiFeO_3$ multiferroics, Mater. Res. Bull. 111 (2019) 93–101.
[31] W. Sun, Z. Zhou, J. Luo, K. Wang, J.F. Li, Leakage current characteristics and Sm/Ti doping effect in $BiFeO_3$ thin films on silicon wafers, J. Appl. Phys. 121 (2017) 064101.
[32] M.S. Bernardo, T. Jardiel, M. Peiteado, F.J. Mompean, M. Garcia-Hernandez, M.A. Garcia, M. Villegas, A.C. Caballero, Intrinsic compositional inhomogeneities in bulk Ti-doped $BiFeO_3$: microstructure development and multiferroic properties, Chem. Mater. 25 (2013) 1533–1541.
[33] C. Gumiel, T. Jardiel, M.S. Bernardo, P.G. Villanueva, U. Urdiroz, F. Cebollada, C. Arago, A.C. Caballero, M. Peiteado, Combination of structural and microstructural effects in the multiferroic response of Nd and Ti co-doped $BiFeO_3$ bulk ceramics, Ceram. Int. 45 (2019) 5276–5283.
[34] M.S. Bernardo, D.G. Calatayud, T. Jardiel, D. Makovec, M. Peiteado, A.C. Caballero, Titanium doping of $BiFeO_3$ ceramics and identification of minor phases by Raman spectroscopy, J. Raman Spectrosc. 48 (2017) 884–890.
[35] H. Yang, C. Zhou, X. Liu, Q. Zhou, G. Chen, H. Wang, W. Li, Structural, microstructural and electrical properties of $BiFeO_3$-$BaTiO_3$ ceramics with high thermal stability, Mater. Res. Bull. 47 (2012) 4233–4239.
[36] M.S. Bernardo, T. Jardiel, M. Peiteado, A.C. Caballero, M. Villegas, Sintering and microstructural characterization of W^{6+}, Nb^{5+} and Ti^{4+} iron-substituted $BiFeO_3$, J. Alloy Compd. 509 (2011) 7290–7296.
[37] J. Rodríguez-Carvajal, Recent advances in magnetic-structure determination by neutron powder diffraction, Phys. B Condens. Matter 192 (1993) 55–69.
[38] T. Roisnel, J. Rodríquez-Carvajal, WinPLOTR: a Windows tool for powder diffraction pattern analysis, Mater. Sci. Forum 378 (2001) 118–123.
[39] M.N. Rahaman, Ceramics Processing and Sintering, Marcel Dekker Inc, New York, 1995.
[40] C. Gumiel, M.S. Bernardo, P.G. Villanueva, T. Jardiel, J. De Frutos, A.C. Caballero, M. Peiteado, Solid state diffusion and reactivity in the multiferroic $BiFeO_3$-$Bi_4Ti_3O_{12}$ composite system, J. Mater. Sci. 52 (2017) 4042–4051.
[41] S.B. Desu, D.A. Payne, Interfacial segregation in perovskites: IV, Internal boundary-layer devices, J. Am. Ceram. Soc. 73 (1990) 3416–3421.
[42] M.A. De la Rubia, M. Peiteado, J.F. Fernandez, A.C. Caballero, J. Holc, S. Drnovsek, D. Kuscer, S. Macek, M. Kosec, Thick film ZnO based varistors prepared by screen printing, J. Eur. Ceram. Soc. 26 (2006) 2985–2989.
[43] M. Peiteado, Y. Iglesias, A.C. Caballero, Sodium impurities in ZnO-Bi_2O_3-Sb_2O_3 based varistors prepared by screen printing, Ceram. Int. 37 (2011) 819–824.
[44] S.D. Desu, D.A. Payne, Interfacial segregation in perovskites: III, Microstructure and electrical properties, J. Am. Ceram. Soc. 73 (1990) 3407–3415.